PNAS RESEARCH ARTICLE | ENVIRONMENTAL SCIENCES

The weekly cycle of photosynthesis in Europe reveals the negative impact of particulate pollution on ecosystem productivity

Liyin He[a,1], Lorenzo Rosa[a,1], David B. Lobell[b,c], Yuan Wang[b], Yi Yin[d,e], Russell Doughty[f], Yitong Yao[d], Joseph A. Berry[a], and Christian Frankenberg[d,g]

Edited by William Schlesinger, Cary Institute of Ecosystem Studies, Millbrook, NY; received April 21, 2023; accepted October 3, 2023

Aerosols can affect photosynthesis through radiative perturbations such as scattering and absorbing solar radiation. This biophysical impact has been widely studied using field measurements, but the sign and magnitude at continental scales remain uncertain. Solar-induced fluorescence (SIF), emitted by chlorophyll, strongly correlates with photosynthesis. With recent advancements in Earth observation satellites, we leverage SIF observations from the Tropospheric Monitoring Instrument (TROPOMI) with unprecedented spatial resolution and near-daily global coverage, to investigate the impact of aerosols on photosynthesis. Our analysis reveals that on weekends when there is more plant-available sunlight due to less particulate pollution, 64% of regions across Europe show increased SIF, indicating more photosynthesis. Moreover, we find a widespread negative relationship between SIF and aerosol loading across Europe. This suggests the possible reduction in photosynthesis as aerosol levels increase, particularly in ecosystems limited by light availability. By considering two plausible scenarios of improved air quality—reducing aerosol levels to the weekly minimum 3-d values and levels observed during the COVID-19 period—we estimate a potential of 41 to 50 Mt net additional annual CO_2 uptake by terrestrial ecosystems in Europe. This work assesses human impacts on photosynthesis via aerosol pollution at continental scales using satellite observations. Our results highlight i) the use of spatiotemporal variations in satellite SIF to estimate the human impacts on photosynthesis and ii) the potential of reducing particulate pollution to enhance ecosystem productivity.

photosynthesis | aerosol | climate mitigation | satellite remote sensing | ecosystem productivity

Significance

The impact of particulate pollution on photosynthesis at continental scales remains uncertain. We report evidence of a widespread negative relationship between photosynthesis and aerosol loading across Europe using space-based observations of solar-induced fluorescence (SIF) that are mechanistically linked to plant photosynthesis. Specifically, we find that 64% of regions in Europe show increased SIF on weekends, when there is more plant-available sunlight due to reduced particulate pollution. Using satellite observational datasets, our findings provide compelling evidence that reducing particulate pollution has the potential to enhance ecosystem productivity by absorbing carbon from the atmosphere.

Efforts to increase ecosystem productivity, with increased CO_2 uptake by plants through photosynthesis, are needed in the coming decades to achieve the goal of net-zero CO_2 emissions later this century (1). Improving air quality is one potential strategy to enhance ecosystem productivity, though its primary motivation is human health benefits. Atmospheric aerosols (also known as particulate matter) are one of the main air pollutants, which originate from both natural sources such as dust, pollen, and sea spray, as well as human activities like industrial emissions, transportation, and agriculture (2). Observations at plot or site scale have identified that two major effects of aerosols on ecosystem productivity are the reduction of total solar radiation reaching the ground for plant photosynthesis and the increase in diffuse radiation and light use efficiency (3–5). However, the potential benefit of the latter is often offset or even reversed by the reduction in total radiation, especially under high aerosol loading (6–12). Meanwhile, aerosols can affect ecosystem productivity through changes in air temperature (Tair), vapor pressure deficit (VPD), soil moisture (SM), etc. (13–18). In some cases, levels of aerosols can suppress crop yields by as much as 30% (12, 19–22) and negatively affect grassland productivity, while their influence on forest productivity varies depending on factors such as plant species, aerosol types, and cloud conditions (4, 10, 11, 23–25). Though these studies have provided valuable insights (8, 9, 26–31), they are often affected by large uncertainties associated with extrapolating the results beyond the experimental conditions. Some studies have used Earth system models but these models may not well represent aerosol-induced climate feedback (6, 10, 32, 33). Therefore, there is a pressing need for large-scale observational studies to comprehensively understand the effects of aerosols on ecosystem productivity.

Recent advancements in satellite technology have greatly improved our ability to continuously track ecosystem productivity on a global scale. The TROPOspheric Monitoring Instrument (TROPOMI), launched in 2017, is particularly noteworthy for its ability to retrieve solar-induced fluorescence (SIF) at a daily frequency and high spatial resolution of 7 × 3.5 km (34). SIF emissions, which are emitted by chlorophyll molecules, exhibit a

Author contributions: L.H. and D.B.L. conceived the study; L.H., L.R., D.B.L., and C.F. designed the study; L.H. and R.D. collected data; L.H. performed data analysis and wrote the paper; Y.W., Y. Yin, and J.A.B. contributed the discussion of method development; L.H. led the interpretation of the results with input from L.R., D.B.L., Y.W., Y. Yin, Y. Yao, J.A.B., and C.F.; and all authors provided feedback on the manuscript.

The authors declare no competing interest.

This article is a PNAS Direct Submission.

[1]To whom correspondence may be addressed. Email: lhe@carnegiescience.edu or lrosa@carnegiescience.edu.

This article contains supporting information online at https://www.pnas.org/lookup/suppl/doi:10.1073/pnas.2306507120/-/DCSupplemental.

Published November 20, 2023.

stronger correlation with plant photosynthesis, as estimated by gross primary productivity (GPP), compared to reflectance-based greenness indices (35–42). Furthermore, SIF emissions at near-infrared bands are hardly affected by high levels of aerosols, which makes SIF retrievals less susceptible to aerosol interference (43). In contrast, high aerosol loading has a larger impact on the reflectance of the red band than the near-infrared band, making greenness indices sensitive to the presence of aerosols (44). Therefore, TROPOMI SIF provides a unique opportunity to capture nearly daily variations in photosynthesis in response to aerosol changes across space.

Satellite measurements provide a practical and reliable method to assess aerosol exposure at a spatiotemporal resolution consistent with SIF observations. Our preferred aerosol index, aerosol optical depth (AOD), measures the amount of sunlight blocked from reaching the surface due to the presence of aerosols in the atmosphere. Here, we use Visible Infrared Imaging Radiometer Suite (VIIRS) AOD at 550 nm, particularly focusing on the weekly cycle, to distinguish between anthropogenic and natural aerosols. Anthropogenic aerosols, which are associated with human activities, are expected to exhibit different patterns on weekends versus weekdays. By adopting this approach, we aim to investigate the impact of human-related aerosols on ecosystem productivity.

Here, we investigate the potential of reducing aerosol pollution to increase ecosystem productivity in Europe. We focus on Europe mainly for three reasons. First, consistent patterns of human activity throughout the week are observed in Europe, as evidenced by lower satellite nitrogen dioxide (NO_2) measurements and human mobility during weekends than on weekdays (*SI Appendix*, Figs. S1–S4). This consistency allows us to use the contrasts of satellite AOD and SIF observations between weekdays and weekends to estimate the sensitivity of ecosystem productivity to aerosol loading. Second, terrestrial ecosystems in Europe are facing significant changes due to global warming (45). However, limited studies have investigated the relationship between air quality and ecosystem productivity in these areas (46). Last, Europe has set an ambitious goal to achieve net-zero CO_2 by 2050 by reducing emissions and offsetting any remaining emissions through carbon sequestration (47). Hence, our findings will have significant policy implications, as we seek to assess how improving air quality can enhance ecosystem productivity.

This study aims to address the following three questions. First, is there a strong negative correlation between SIF and AOD, indicating that aerosol loading plays a significant role in plant photosynthesis? Second, how does the effect of AOD on SIF vary across different regions? Third, how much is the potential increase in net ecosystem productivity (NEP) that could be achieved if AOD levels were reduced? Here, NEP is defined as the difference between ecosystem carbon uptake through GPP and carbon release through ecosystem respiration with certain processes like volatiles, exudates, symbioses, and herbivory excluded from consideration.

To answer these questions, we devise the following strategy. First, we leverage satellite AOD to identify a widespread weekly pattern across Europe, with lower levels on weekends compared to weekdays, presumably due to reduced industrial and transport activities. We also observe higher SIF, a proxy for plant photosynthesis (or GPP), on weekends compared to weekdays. Second, using these weekly pattern signals, we assess the sensitivity of SIF to ambient AOD changes, accounting for regional variations in vegetation coverage and climate factors. Third, we determine the sensitivity of GPP to AOD changes for major land cover types in Europe using biome-specific calibration coefficients for GPP-SIF. We also estimate the corresponding changes in NEP to changes in AOD based on the observed proportional relationship between NEP and GPP for each biome. Finally, we estimate the potential NEP increase under two plausible AOD reductions scenarios, including i) the difference in AOD between the 3-d minimum and the average levels observed in a week, and ii) the difference in AOD between the COVID-19 pandemic year and the preceding or following years when human activities returned to normal. It should be noted that the calculated NEP enhancement reflects the possible short-term gains in ecosystem productivity from hypothetical air-quality improvement, while assuming the absence of significant physiological or ecological shifts within the ecosystem and no longer-term adjustments in carbon allocation or ecosystem properties. We validate our findings using data from 29 eddy covariance sites across Europe, which confirm increased GPP on weekends compared to weekdays and a strong correlation between satellite SIF and eddy covariance GPP. Overall, our findings provide a continent-scale estimate of marginal increases in NEP and GPP achievable through reductions in aerosol pollutants.

Results

Widespread SIF Enhancement during Weekends across Europe. We observed widespread enhancement of SIF, during the weekends in 64% of European regions (Fig. 1*A*). The variation of SIF was linked to changes in atmospheric aerosol loadings over the course of the week. We observed a decrease in AOD during the weekend in most regions of Europe (Fig. 1*B*). This confirms previous studies that reported reductions in AOD on weekends in Central Europe using ground or satellite measurements (48–50). We also observed that NO_2 measured by TROPOMI (*SI Appendix*, Fig. S7) decreased in parallel with the decrease in AOD as expected if both were due to fewer human activities such as less industrial and transportation emissions on weekends. In some regions, such as Eastern Europe, AOD exhibited irregular fluctuations on a weekly cycle, which might be attributed to natural processes such as wildfires, dust storms, and the transport of aerosols (48, 50). Overall, the predominant decreases in AOD during the weekends led to a net increase in the amount of sunlight reaching the surface of the Earth, which resulted in an enhancement of absorbed photosynthetically active radiation (APAR) (Fig. 1*C*). Here, APAR was derived from moderate-resolution imaging spectroradiometer (MODIS) satellite data (*Methods*). An increase in APAR, which represents the portion of sunlight absorbed by plants for photosynthesis, would stimulate photosynthesis below the light saturation point. We also investigated the impact of clouds on APAR but found no consistent pattern of cloud optical thickness at the weekly scale (*SI Appendix*, Fig. S8). In addition, we used the fifth-generation European Centre for Medium-Range Weather Forecasts (ECMWF) reanalysis (ERA5) climate data and found a general increase in air temperature and VPD when AOD is lower on weekends, while SM tends to decrease (*SI Appendix*, Fig. S9).

Mechanism of Photosynthesis Enhancement over Weekends. The influence of the difference between less polluted and polluted air, which underlies the observed changes in SIF, is illustrated in Fig. 2*A*. We used a structural equation model (SEM) (51) to analyze causal relationships between aerosols, climate factors, and SIF on a weekly scale (Fig. 2*B*). In the model, we hypothesized that aerosols have a direct effect on the amount of sunlight absorbed by plants, thus affecting SIF. Additionally, aerosol can alter the energy balance at the surface, thereby affecting air temperature. Changes in air temperature can further impose direct or indirect effects on other factors, such as VPD and SM. A set of multiple linear regression models was constructed based on these variables and connections identified. The partial regression coefficients,

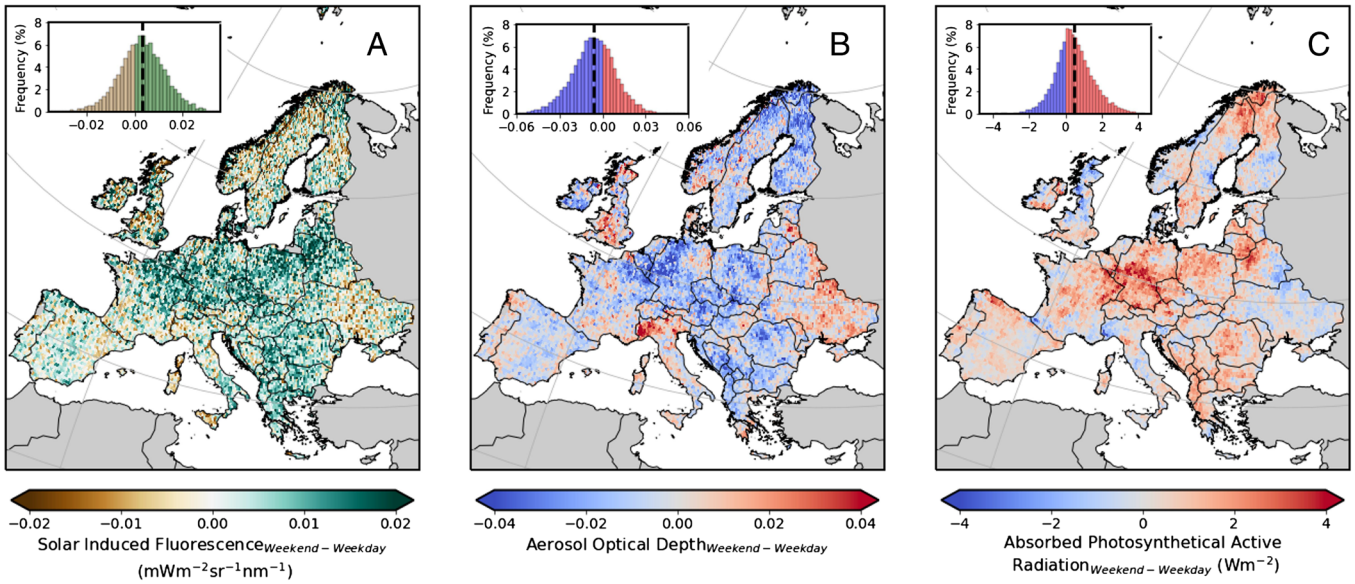

Fig. 1. Weekend minus weekday SIF, AOD, and APAR. The maps show the difference of satellite observed (*A*) SIF, (*B*) AOD, and (*C*) APAR between weekend and weekday in Europe during 2018, 2019, and 2021. We excluded the year 2020 because human activities were greatly affected by the COVID-19 pandemic, leading to a less pronounced or even reversed weekly pattern shown in *SI Appendix*, Fig. S5. The insert histogram shows the distribution of the corresponding variable, with the black dahsed line representing the median. The percent changes of each variable are shown in *SI Appendix*, Fig. S6. To determine the difference between weekends and weekdays for a specific variable each week, we calculated the difference between the average values during weekends (Saturday and Sunday) and weekdays (Monday–Friday). We then aggregated these weekly differences into an average pattern during 2018, 2019, and 2021 (*Methods*).

referred to as path values (PV), were determined based on SEM to indicate the causative strength of each connection.

Using SEM, we found a strong negative effect (PV = −0.52) of AOD on APAR (Fig. 2*B*). On a weekly scale, the variations in SIF are mainly explained by variations in APAR (PV = 0.31) (Fig. 2*B*). While other climate factors, e.g., air temperature, VPD, and SM might also affect photosynthesis, their effects on SIF were less significant. Our SEM analysis suggests that SIF is highly sensitive to variations in AOD. Generally, on weekends, a decrease in AOD leads to an increase in the amount of light reaching the plants, resulting in an enhancement of SIF, particularly when the ecosystem is below the light saturation point.

Sensitivity of SIF to Aerosol Loadings Based on Weekly Pattern Signals. We derived the spatially explicit pattern of the sensitivity of SIF to AOD. Multilinear regression was employed to model the relationship between SIF and various independent variables including AOD, air temperature, VPD, SM, and vegetation fraction (*Methods*). The analysis was based on weekly pattern signals, which means that all variables are represented as the difference between weekends and weekdays. Using this weekly pattern signals approach, we minimized the impact of climate variables and better isolated the effect of aerosol pollution on photosynthesis.

We found a widespread negative response of SIF to AOD across Europe (Fig. 3). This suggests that an increase in AOD generally leads to a decrease in SIF. It should be noted that the sensitivity of SIF to AOD is generally not significant for most grid cells in high latitudes (e.g., >65°N) due to less vegetation coverage and noise in SIF signals. The diverse responses of SIF to AOD that we observed suggest varying impacts of aerosols on photosynthesis. This impact, known as the diffuse fertilization effect, is influenced by factors such as radiation level and aerosol loading (6). The benefits of diffuse radiation become more pronounced with higher radiation levels (52) but could potentially constrain photosynthesis in high-latitude ecosystems which are usually light limited (53). Previous studies have found that there is an optimal threshold of AOD, represented by a "bell curve" pattern, where increases in AOD would enhance photosynthesis below the optimal point, but have a negative effect above this point (8, 10). Moreover, the influence of diffuse fertilization varies across leaf area index and plant species (52). For example, closed canopies with clustered leaves, such as temperate broadleaf forests, tend to respond positively to an increase in diffuse radiation (25), whereas boreal needleleaf forests and open canopies, such as grasslands, may not respond or even respond negatively (11, 26, 53). To unravel the complex mechanisms behind the SIF–AOD relationship, future studies could employ higher-frequency SIF signals from ground-based measurements or geostationary satellite observations.

Reducing Aerosol Pollution Promotes Photosynthetic Carbon Uptake. The above findings of widespread enhancement of SIF on weekends and negative response of SIF to AOD suggest that reducing aerosol pollution could lead to increased photosynthesis. While there may be nonlinearity between SIF and photosynthesis at fine or short timescales due to the decoupling of fluorescence from photosynthetic carbon uptake, satellite SIF is generally linearly correlated with photosynthesis due to the integration of canopy processes at large scales (54, 55). Based on the analysis of 29 eddy covariance sites, we found a robust linear correlation between daily TROPOMI SIF and eddy covariance photosynthesis estimates across a range of biomes (*SI Appendix*, Fig. S12). Notably, the magnitude of the GPP-SIF slope in the range of 9 to 13 was consistent with recent findings (56, 57). Additionally, we observed that eddy covariance photosynthesis estimates exhibit comparable weekly patterns with SIF, e.g., with around 5% weekend enhancement over central Europe (*SI Appendix*, Fig. S13). These findings support the use of the observed relationship between SIF and AOD as a proxy for the relationship between photosynthesis and AOD. This surrogate relationship can be employed to provide insights into the possible short-term benefits of NEP resulting from air pollution mitigation.

We then estimated the increase of NEP at the country level in Europe based on the observed sensitivity of SIF to AOD in Fig. 3,

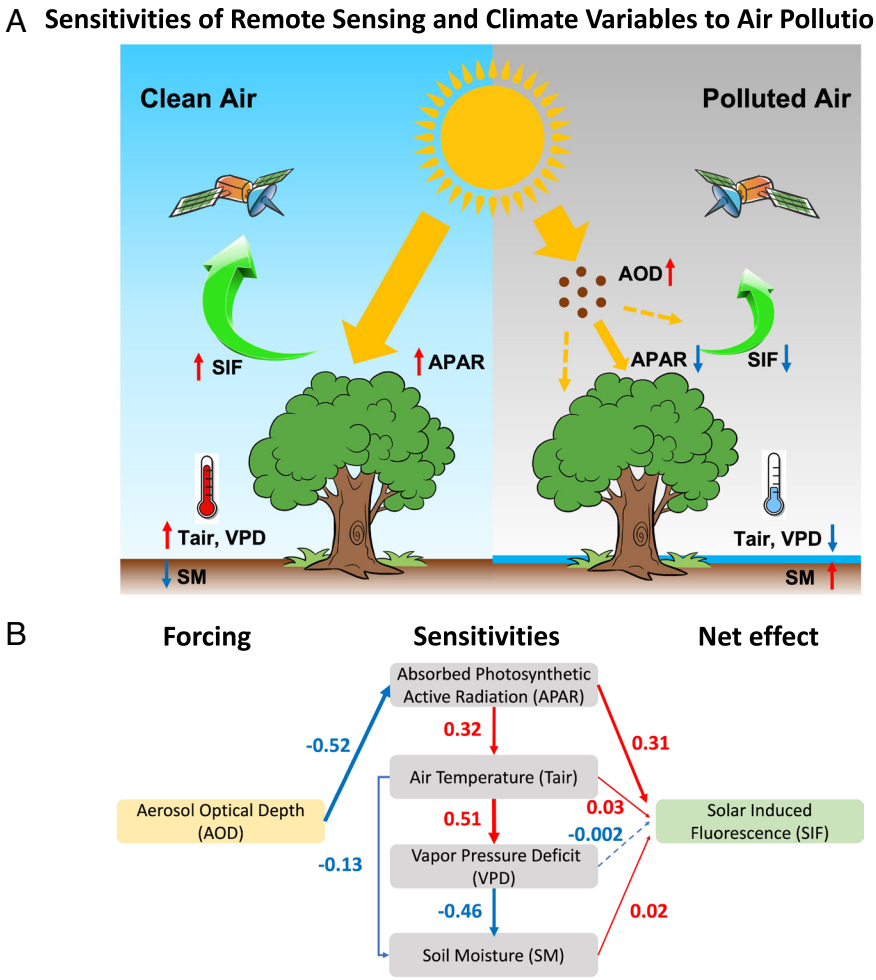

Fig. 2. The aerosol–solar induced fluorescence feedback on a weekly scale. We show (*A*) the schematic depiction of aerosol effects on SIF and (*B*) SEM representing the effects of aerosol on solar induced fluorescence through its influences on APAR, Tair, VPD, and SM. The difference of each variable between weekend and weekday is calculated and then normalized by subtracting the mean and dividing by the SD. The solid lines represent significant relationships (*P*-value < 0.01). PV are shown alongside each arrow, indicating the causative power of each connection, with 1 and −1 indicating the maximum and minimum influence, respectively. Arrow widths are proportional to the PV. Red represents positive path correlation, whereas blue represents negative path correlation.

along with biome-specific calibration coefficients for SIF, GPP, and NEP (*Methods*). For each country, we assessed the net photosynthetic carbon uptake, which was calculated as 3.67 times NEP to convert units of carbon to units of CO_2, in three major biome groups in Europe including forests, grasslands/savannas/shrublands, and cropland.

Two clean-air scenarios are considered in the study. In the first scenario (scenario 1), the aerosol level is reduced to the weekly minimum 3-day at each pixel. This represents a hypothetical scenario in which aerosol pollution is reduced to the lowest levels observed over a week. In the second scenario (scenario 2), the aerosol level is reduced to the level seen during the COVID-19 period in 2020. This scenario represents the lower level of aerosols due to decreased human activities, such as industrial and transportation activities, caused by the pandemic and related policies (58).

As shown in Fig. 4, Europe has the potential of an annual total of 49.7 (90% confidence interval: 44.9 to 52.8) and 40.9 (CI: 37.3–40.0) Megatons (Mt) additional net CO_2 uptake by ecosystems in scenario 1 and scenario 2, respectively. We found that forests, grasslands/savannas/shrublands, and croplands have a similar potential for increased carbon uptake, contributing 34%, 38%, and 28%, respectively (Fig. 4). In scenario 1, the country with the largest potential is France, with 5.2 (CI: 4.9–5.5) Mt additional CO_2 uptake per year. In France, grasslands/savannas/shrublands contribute the most with 52%, while croplands and forests contribute 30% and 18%, respectively. Other countries with notable potential include Ukraine, Spain, and Italy, with potentials of 4.2 (CI: 3.1–5.2), 3.7 (CI: 3.3–4.0), and 3.5 (CI: 3.2–3.8) Mt annual total additional CO_2 uptake per year, respectively. When normalized by the country's total area, Croatia, Slovenia, and Bulgaria are the top three countries with potential (Fig. 4). In scenario 2, France still has the largest potential with 5.2 (CI: 4.9–5.5) Mt additional CO_2 uptake per year. Other countries with notable potential include Germany, Poland, and Italy, with potentials of 4.1 (CI: 3.8–4.4), 3.5 (CI: 3.1–3.8), and 2.7 (CI: 2.4–3.0) Mt annual total additional CO_2 uptake per year, respectively. When normalized by country's total area, Croatia, Slovenia, and Bosnia and Herzegovina are the top three countries with potential. We also assessed the potential for ecosystems to absorb an additional annual total of 176 (CI: 148–165) and 138 (CI: 125–146) Mt CO_2 in scenarios 1 and 2, respectively, if respiration were excluded (*SI Appendix*, Fig. S14).

Discussion

In this study, we used satellite remote sensing measurements to investigate the effects of aerosols on photosynthesis (or GPP) across Europe. Then, we employed modeling to estimate possible

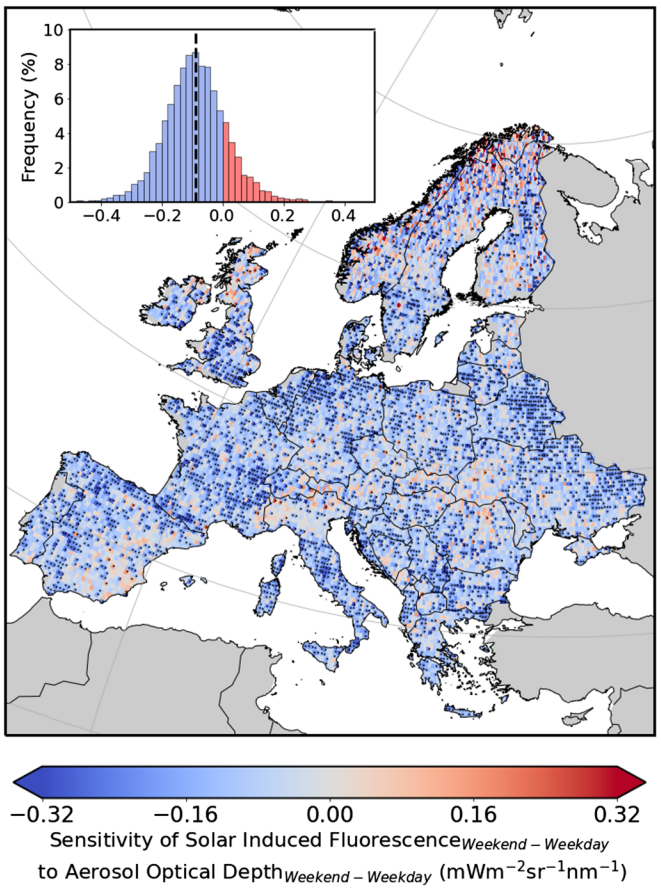

Fig. 3. Sensitivity of solar induced fluorescence to aerosols. Spatial map of the sensitivity of solar induced fluorescence to 1 unit increase in AOD in Europe derived from weekly patterns, which refers to weekend minus weekday signals, during 2018, 2019, and 2021. The grids marked with black dots indicate that the regression coefficient is significant with *P*-value < 0.05. The histogram shows the distribution of the derived sensitivity. The estimated standard error (SE) of the sensitivity is shown in *SI Appendix*, Fig. S10, which is used in uncertainty analysis afterwards. Relative changes of solar induced fluorescence (unit: %) responding to AOD is shown in *SI Appendix*, Fig. S11.

short-term effects on NEP. We found that there is a widespread SIF enhancement during weekends in Europe. This enhancement is associated with a decrease in AOD, which is likely due to fewer human activities such as industrial and transportation emissions on weekends. The decrease in AOD leads to an increase in the amount of sunlight reaching the surface of the Earth, which results in an enhancement of plant-available photosynthetically active radiation. Such increased radiation is particularly beneficial for plants in light-limited regions, such as high-latitude ecosystems, to enhance their photosynthesis. By leveraging the temporal gradient between weekends and weekdays, we minimized the influence of climate variations and isolated the sensitivity of SIF to AOD. Our findings reveal that most regions exhibit negative responses, suggesting that reducing aerosol pollution caused by human activities could enhance photosynthetic carbon gain in light-limited ecosystems. We further estimated that Europe has the potential for an annual total of net 50 and 41 Mt additional CO_2 uptake by ecosystems if aerosol levels are reduced to the weekly minimum 3 d at each pixel or to the level seen during the COVID-19 period in 2020, respectively. Our results highlight that reducing aerosol pollution could have a significant positive impact on ecosystem productivity and carbon sequestration.

Our findings have significant implications for crop productivity. We show substantial potential for cropland carbon uptake in countries such as France, Ukraine, Poland, and Germany, as shown in Fig. 4. Additionally, we observed a 2.4% decrease in SIF over cropland with an increase of 0.1 unit in AOD, as shown in *SI Appendix*, Fig. S11, which is consistent with the magnitude estimated by 2–6% crop yield reduction responding to a 0.1 increase of AOD in China (21). Meanwhile, other studies have shown that aerosols have negatively impacted 11–23% of soybean and maize from 1980 to 2019 in the United States (22) and 6% from 1980 to 2010 for rain-fed rice in India (19).

Our findings have implications for carbon sequestration, particularly considering the European Union's commitment to reach net-zero CO_2 emissions by 2050 (47). The European Union is planning to set up a certification system for carbon removals and aims to capture ~500 Mt of CO_2 from the atmosphere annually through methods such as direct air capture, bioenergy with carbon capture and storage (BECCS), and carbon sequestration in forests, soil, and wetlands. Recent studies have estimated that agricultural residues and waste biomass throughout Europe could capture up to 250 Mt of CO_2 per year through BECCS technologies (59, 60). Our study finds that improved air quality could lead to the removal of 41 to 50 Mt CO_2 per year through increased photosynthesis. However, it is important to note that this atmospheric carbon removal may not be permanent, as it can be released through events such as fires, pests, windstorms, and deforestation (61). To ensure long-term carbon sequestration, the captured carbon in crops and forests can be utilized as a feedstock for BECCS, enabling permanent sequestration in suitable geological formations (61). Enhancing biomass availability, supported by improved air quality, plays a crucial role in achieving net-zero emissions through BECCS and facilitates the decarbonization of hard-to-abate industries such as the chemical industry and aviation (62, 63). Therefore, up to 300 Mt of CO_2 per year (or 60%) of carbon dioxide removal needs could be used to mitigate hard-to-abate emissions in Europe if there is a permanent storage of biogenic CO_2. It is also important to note that while reducing aerosol pollution has the potential of negative radiative forcing through photosynthetic carbon gain, however, in the short term, this effect may be counteracted by the increase in air temperature resulting from changes in the surface radiation budget. For example, we observe a regional average warming of 0.02 K over the weekend with less aerosol pollution as shown in *SI Appendix*, Fig. S9.

Our results suggest some opposing effects of geoengineering strategies. Injecting aerosols into the atmosphere has emerged as a proposed geoengineering strategy aimed at mitigating the rise in global temperatures by reducing incoming solar radiation (64). This approach involves releasing fine particles into the atmosphere to create a temporary shield that reflects sunlight back into space. While this method has the potential to curb the increase in global temperature, it also raises significant concerns (14). Our findings suggested that increased aerosol concentrations may result in adverse consequences such as decreased crop yields and reduced carbon uptake by terrestrial ecosystems in mid-high latitude regions. These unforeseen results underscore the intricate nature and inherent uncertainties associated with manipulating the Earth system on a large scale, highlighting the need for cautious and comprehensive evaluations when considering geoengineering as a potential solution to global climate challenges.

Our proposed approach by comparing satellite-observed plant-emitted signals on clean versus polluted days offers a unique and useful framework to understand the impact of aerosols on ecosystem productivity. This method can be adapted in regions with a less regular weekly cycle of air pollution or human activities (*SI Appendix*, Fig. S1) due to the atmospheric transport of aerosols or irregular industrial, commercial, and leisure activities over the

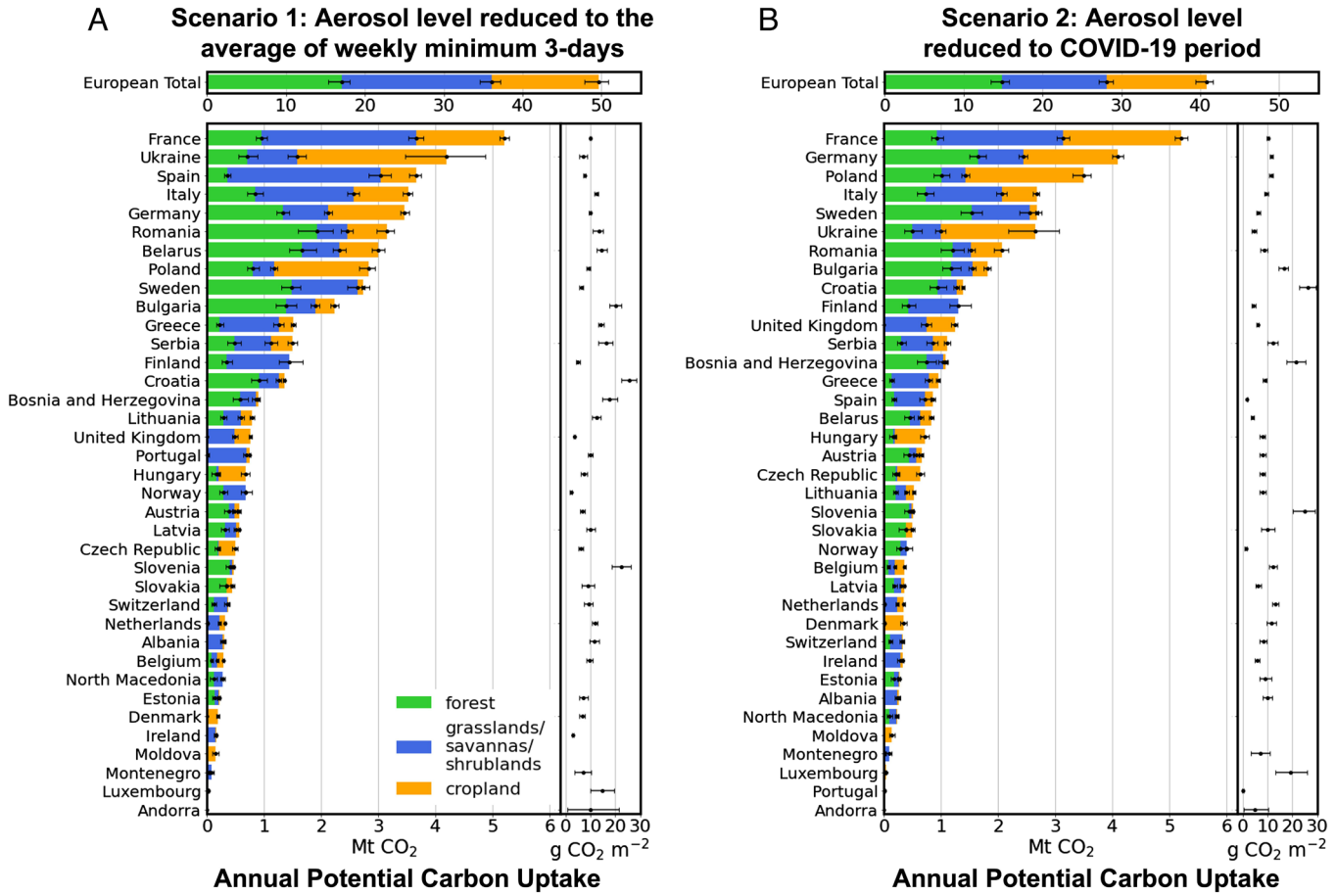

Fig. 4. Annual net photosynthetic carbon gain through aerosol pollution reduction in two pollution mitigation scenarios. The increase in country-level annual net carbon uptake under pollution mitigation scenarios in Europe, with aerosol level reduced to (*A*) the average of weekly minimum 3 d and (*B*) COVID-19 period, represented by year 2020. Green, blue, and yellow bars represent the increase of annual carbon uptake by forest, grasslands/savannas/shrublands and cropland, respectively. To estimate the range of estimated values, we consider the uncertainties associated with SIF sensitivities to AOD, the conversion factor of SIF to GPP, the conversion factor of GPP to NEE, and the definition of the growing season based on the fraction of photosynthetically active radiation (fPAR). We employed a bootstrap approach, resampling the data 1,000 times. The central estimates are represented by the median, while the upper and lower bounds correspond to the 95th and 5th percentiles, respectively (*Methods*). The corresponding annual total photosynthesis increases through aerosol pollution reduction in two pollution mitigation scenarios is shown in *SI Appendix*, Fig. S14.

course of the week. In such cases, we could use alternative reference points by using air-quality data or national holidays to distinguish between clean and polluted days. Recent efforts have been made to use the year 2020, during the COVID-19 pandemic, as a reference to observe that China and India appear greener in 2020 due to decreased AOD, though separating meteorological effects can be challenging (65, 66). By understanding the complex relationships between human activity, air quality, and ecosystem productivity, we can develop more effective policies and practices to mitigate the negative effects of air pollution and enhance ecosystem productivity.

While we conduct a rigorous uncertainty analysis (*Methods*) to determine the confidence interval of our estimates of photosynthetic carbon gain (Fig. 4), there are three major factors that have not been fully considered in the above analyses. First, while we can estimate GPP using SIF observations, the modeling of NEP remains subject to uncertainties due to the limitations of satellite measurements in tracking ecosystem respiration. For example, the reduced aerosol pollution could potentially increase temperature, thereby enhancing ecosystem respiration. At the flux tower scale, we observe an increase in both GPP and ecosystem respiration during weekends compared to weekdays for most of the sites (*SI Appendix*, Fig. S15). However, the magnitude of the increase in GPP is generally larger than that of ecosystem respiration, resulting in a net increase in NEP (*SI Appendix*, Fig. S15). At the continental scale, since remote sensing techniques only capture GPP and not ecosystem respiration, we approximate the change in ecosystem respiration due to increased temperature using a simplified model (*SI Appendix*, *Supplementary Text S1*). Nevertheless, the modeled changes in ecosystem respiration are relatively minor compared to the observed increase in SIF during weekends. Further research could explore a more comprehensive analysis of the effects of AOD on ecosystem respiration, incorporating additional flux tower sites representing diverse plant species and climate zones. Second, the use of the minimum 3-day period within a week as a reference clean scenario may be conservative due to the presence of residual aerosols in the upper atmosphere. These aerosols do not dissipate immediately and can persist for several days. The lifetime of aerosols is subject to removal processes involving wet scavenging or gravitational settling, which are further determined by factors such as aerosol size, composition, atmospheric conditions, and the presence of precipitation. Since our study employs AOD as a proxy for human activity intensity, the prolonged lifespan of aerosols can result in elevated AOD values

even during periods of reduced human activity. This may lead to an overestimation of AOD during presumed less polluted days within the week, leads to a potential underestimate of the actual carbon gain when considering the minimum 3-day period as a reference clean scenario. Third, we employ satellite-measured SIF, which captures the emitted SIF from the top of the canopy, to investigate the relationship between photosynthesis and aerosols. However, the effects of aerosols-induced diffuse light are known to be more related to shaded leaves at the lower canopy levels. Future research could explore the mechanisms underlying how SIF responds to diffuse light using in-situ measurements.

In summary, our study demonstrates the potential of satellite SIF as a useful tool to investigate the impacts of aerosols on photosynthesis in light-limited scenarios at the continental scale. It is remarkable that despite the challenges posed by satellite measurement noise, repeated measurements demonstrate the ability to resolve statistically significant differences in SIF signals and presumably photosynthesis. SIF can further serve as a global "light sensor" for estimating aerosol impacts on radiation balance and temperature, which are important for understanding global climate change accompanied by anthropogenic activities. The consistent and widespread negative impact of AOD on SIF across diverse conditions reported here represents a significant step forward in understanding the widespread impact of air pollution on ecosystem productivity.

Methods

Satellite Solar-induced Chlorophyll Fluorescence Data. We use satellite solar-induced chlorophyll fluorescence, or SIF, as a proxy for photosynthesis at a large scale. The high spatial resolution (7 km × 3.5 km) and near-global daily coverage of TROPOMI SIF allow us to study the variations of SIF at a high spatiotemporal resolution. TROPOMI is a multiband imaging grating spectrometer that is aboard the European Sentinel-5 Precursor satellite launched on 13th October 2017 (34). TROPOMI covers the far-red part of the SIF emission spectrum, specifically in the range of 743–758 nm, which is a subset of TROPOMI's band 6 (725–775 nm). The TROPOMI instrument provides SIF measurements at local time of 13:30. We then apply a daily correction factor to convert the instantaneous SIF measurements into daily averages to account for the length-of-day and the variability of the solar zenith angle (37). Recent studies have shown strong correlation, e.g., linear relationship between TROPOMI SIF and photosynthesis at canopy and regional scales across different types of ecosystems (34, 56, 67–69). In this study, we utilize the well-established TROPOMI SIF product developed by Köhler et al. (34) to investigate the relationship between aerosols and photosynthesis across Europe. Here, we try to include as many meaningful SIF measurements as possible by applying a filtering to include observations with cloud fractions less than 80% (34). To test the robustness of our results, we conduct additional analysis with cloud filtering at 60% and 40%, as shown in *SI Appendix*, Fig. S16 and find that the spatial patterns of the differences in SIF during weekends and weekdays are consistent with those in Fig. 1. Additionally, we investigate whether these patterns are affected by variations in the phase angle but find no consistent patterns in the patterns over the course of the week as shown in *SI Appendix*, Fig. S17. To reduce the impact of bidirectional reflectance and aerosol-related retrieval uncertainties on the signal, we also employ relative SIF, which refers to SIF normalized by the continuum-level NIR-reflected radiance. Our findings in *SI Appendix*, Fig. S18 reveal a similar pattern in Fig. 1, indicating that the widespread decrease in SIF is primarily attributed to reductions in APAR, rather than being influenced by aerosol-induced signal attenuation. To consolidate our results, we use an alternative SIF product derived from TROPOMI data with a different retrieval algorithm (70), and find a consistent spatial pattern of widespread increased SIF across Europe on weekends using TROPOSIF (*SI Appendix*, Fig. S19). We aggregate TROPOMI SIF at a daily resolution of 0.25 degrees to match the resolution of the AOD and climate data.

Satellite AOD Data. AOD is used as a proxy for aerosol pollution, as it measures the extinction of light due to the presence of aerosols in the atmosphere. The VIIRS on board the Suomi National Polar-orbiting Partnership (SNPP) is a sensor with 22 spectral bands that cover a range of wavelengths from 412 to 12,050 nanometers with a moderate spatial resolution of 750 m for the visible and infrared bands. We use AOD products generated using the Enterprise Processing System (EPS) algorithm, which has made significant improvement over the previous Interface Data Processing Segment (IDPS) algorithm (71). We use daily AOD at 550 nm for accurate tracking of fine particulate matter caused by human activities, which is a key component of aerosol pollution. Previous studies have found good agreement between VIIRS EPS AOD and ground-based measurements (71).

Climate Data. We use climate data from the fifth-generation ECMWF reanalysis (ERA5), including hourly air temperature, VPD, and SM at the upper 7 cm at 0.25 degrees. These data are aggregated to daily averages for comparison with satellite SIF and AOD measurements. We calculate the APAR by multiplying the 8-d 500-m fraction of photosynthetically active radiation (fPAR) by the 3-h 0.05-degree photosynthetic active radiation (PAR) from MODIS products. We then aggregate APAR to 0.25 degrees to match the resolution of the other datasets used in the study.

Eddy Covariance Flux Measurements. To investigate whether the weekend increase in TROPOMI SIF is related to an increase in photosynthesis, we compare the difference between weekend and weekday TROPOMI SIF with GPP estimated from eddy covariance flux measurements. We use daily GPP from the ICOS (Integrated Carbon Observation System) (72), which has undergone a standardized quality control and gap-filling process using a consistent pipeline (73). The average of GPP estimates from the night and daytime partitioning methods (GPP_DT_VUT_MEAN and GPP_NT_VUT_MEAN) is used for the analysis. We select 29 sites representing major ecosystems across Europe from 2018 to 2021 (*SI Appendix*, Table S1). We exclude cropland sites due to different management activities, which makes it difficult for a direct comparison with satellite SIF at a coarse resolution.

Derivation of the Difference between Weekend and Weekday. To determine the difference in SIF between weekends and weekdays, we compare the average SIF values during weekends (Saturday and Sunday) with those during weekdays (Monday–Friday). In each weekly cycle, we calculate weekend SIF using data from four consecutive weekend days, whereas weekday SIF is derived from the average SIF over the five weekdays between these two weekends. This approach allows us to make the sample size more comparable and eliminate the effects of solar geometry on SIF signals. The increase in solar angle before the summer solstice in the Northern Hemisphere and the decrease afterward, and vice versa for the Southern Hemisphere, can affect the amount of radiation received by vegetation and thus SIF signals. We also use this approach to derive the difference between weekend and weekday values for other variables, such as AOD and climate data. For regional-scale analysis, we only include pixels for a given day where all satellite remote sensing and climate reanalysis data are available. For the comparison of satellite SIF with eddy covariance GPP, we use pixels at the 0.25-degree grid cell where the flux tower is located and keep those days when both measurements are available. For a specific variable of a given year, there are approximately 52 wk, which results in 52 sets of values for the comparison of weekend and weekday values.

Statistical Analysis. We use linear regression at the pixel level to assess the spatially explicit sensitivity of SIF to aerosol. The equation used for this analysis is as follows:

$$\Delta SIF = \beta_{SIF-AOD} \times \Delta AOD + \beta_{SIF-Tair} \times \Delta Tair + \beta_{SIF-VPD} \times \Delta VPD + \beta_{SIF-SM} \times \Delta SM + \beta_{SIF-fPAR} \times fPAR, \quad [1]$$

where ΔSIF, ΔAOD, $\Delta Tair$, ΔVPD, and ΔSM represent the difference between weekend and weekday values for SIF, AOD, Tair, VPD, and SM, respectively. fPAR is included to represent vegetation fraction in each grid cell. The growing season is considered by including only areas where fPAR is greater than 0.2 at each week. APAR is not included in the equation because of the strong linear relationship between AOD and APAR. The approach of using the difference between weekends and weekdays, instead of absolute values, helps to control for natural climate variations caused by long-term atmospheric processes. This approach also removes the effect of air

temperature seasonality and phenology that may occur over time. For example, the seasonal cycle of SIF and air temperature may be similar, with both being high in the summer. By removing these climate and phenology factors, we can more accurately isolate the impact of AOD on SIF. The observed relatively linear relationship between ΔSIF and ΔAOD at the continent level (*SI Appendix*, Fig. S20) supports the validity of our linear regression framework in this study.

Estimate of Ecosystem Productivity Increases from Aerosol Reduction. To estimate the increase in SIF for a counterfactual scenario of low AOD, we consider two scenarios. In the first scenario (scenario 1), the aerosol level is reduced to the minimum levels observed within a 3-d period in a week, representing a hypothetical situation in which aerosol pollution is reduced to the lowest levels observed within a week. In the second scenario (scenario 2), the aerosol level is reduced to the level seen during the COVID-19 period in 2020, reflecting the decrease in human activities such as industrial and transportation activities (58). These two scenarios are considered as aggressive measures to decrease AOD and represent the upper limit of near-term potential for reducing AOD. A more extreme scenario, in which all locations have zero AOD, was not considered as it is not a realistic scenario due to the presence of nonanthropogenic aerosols such as dust or sea salt aerosols. Additionally, it would exceed the range of data used to estimate the regression.

$$\text{Scenario 1} \quad AOD_{dif} = AOD_{min,3d} - AOD_{avg}, \qquad [2]$$

$$\text{Scenario 2} \quad AOD_{dif} = AOD_{2020} - AOD_{avg}, \qquad [3]$$

where AOD_{avg} and $AOD_{min,3d}$ are the average level and the minimum 3-d observed AOD values, respectively, over the study period including 2018, 2019, and 2021. AOD_{2020} represents the average AOD value during 2020 at each grid cell.

The estimated ordinary least squares (OLS) regression coefficient $\beta_{SIF-AOD}$ in Eq. **1** represents the expected change in plant-emitted SIF for a unit change in AOD. Using this coefficient, we can calculate the change in SIF under a low AOD scenario, described as

$$SIF_{dif} = \beta_{SIF-AOD} \times AOD_{dif}. \qquad [4]$$

To estimate the impact of SIF change on ecosystem productivity, we consider a linear relationship between net ecosystem exchange (NEE), gross primary production (GPP), and SIF, where by definition NEE is the negative of NEP. Specifically, we assume that NEE is directly proportional to GPP, and GPP is directly proportional to SIF, as supported by previous studies (36, 39, 74, 75). Therefore, we can write the relationships as

$$NEE = \beta_{NEE-GPP} \times GPP + \beta_0, \qquad [5]$$

$$GPP = \beta_{GPP-SIF} \times SIF, \qquad [6]$$

where $\beta_{NEE-GPP}$ and β_0 are the slope and intercept for the linear regression between NEE and GPP, respectively. $\beta_{GPP-SIF}$ is the scaling factor of SIF to GPP. We determine $\beta_{NEE-GPP}$ and β_0 for each land cover type using state-of-art global NEE and GPP from FLUXCOM datasets (*SI Appendix*, Fig. S21), which are upscaled from flux tower observations, driven by a variety of machine learning methods and remote sensing observations, such as NDVI and EVI (76). While FLUXCOM has been known to overestimate the global land carbon sink, its representation of carbon fluxes in Europe is considered relatively reliable due to the abundance of flux towers in the region (76). Recent studies have revealed a linear correlation between TROPOMI SIF and flux tower GPP measurements, enabling us to infer GPP based on SIF (56, 57, 77). The scaling factor $\beta_{GPP-SIF}$ is taken from Turner et al. (57), with a value of 9.1 ± 0.2 for grassland and 11.0 ± 0.2 for other species. The reported SIF–GPP relationships have units of (gC m^{-2} d^{-1})/(mW m^{-2} sr^{-1} nm^{-1}). We use biome classifications from the MODIS MCD12Q1 V6 data product, which provides the International Geosphere–Biosphere Program (IGBP) land cover type classification at a resolution of 500 m. We grid it to 0.25 degrees to match the resolution with other datasets.

The difference of NEE in a counterfactual low AOD scenario at each location, e.g., grid cell, can be expressed as

$$\begin{aligned} NEE_{dif} &= \beta_{NEE-GPP} \times GPP_{dif} = \beta_{NEE-GPP} \times \beta_{GPP-SIF} \times SIF_{dif} \\ &= \beta_{NEE-GPP} \times \beta_{GPP-SIF} \times \beta_{SIF-AOD} \times AOD_{dif}. \end{aligned} \qquad [7]$$

The unit of NEE_{dif} is gC m^{-2} d^{-1}, which can then be aggregated at the country level and converted to annual photosynthetic carbon changes, considering the growing season length and the country area.

$$\text{Annual Photosynthetic Carbon Gain}_c = -\sum_i^n NEE_{dif,i} \times Area_i \times GSL_i \times 3.67, \qquad [8]$$

where i represents the grid cell belonging to the country c, GSL represents the number of days during the growing season which is defined as multi-year averaged fPAR during 2018 to 2021 exceeds a threshold (denoted as $fPAR_{growing}$), and $Area$ represents the grid cell area. We use 3.67 to convert units of carbon to units of CO_2, which is the commonly used unit for measuring carbon emissions.

Uncertainty Analysis. We provide upper and lower bounds of annual photosynthetic carbon gain by considering uncertainties associated with four parameters at each grid cell, including $\beta_{SIF-AOD}$, $\beta_{GPP-SIF}$, $\beta_{NEE-GPP}$ and $fPAR_{growing}$. We include $fPAR_{growing}$ to account for the length of the growing season because reductions of AOD during nongrowing seasons would not lead to photosynthetic carbon gain. We conduct 1,000 bootstrap iterations to sample parameter spaces. For each bootstrap, we perform the following sampling:

$$\beta_{SIF-AOD} \sim Normal(\beta_{SIF-AOD}, \ \sigma\beta_{SIF-AOD}),$$

$$\beta_{GPP-SIF} \sim Normal(\beta_{GPP-SIF}, \ \sigma\beta_{GPP-SIF}),$$

$$\beta_{NEE-GPP} \sim Normal(\beta_{NEE-GPP}, \ \sigma\beta_{NEE-GPP}),$$

$$fPAR_{growing} \sim Normal(0.2, \ 0.05).$$

$\beta_{SIF-AOD}$ is determined as the OLS in Eq. **1** (Fig. 3) and $\sigma\beta_{SIF-AOD}$ represents the associated standard error (SE) of the coefficient (*SI Appendix*, Fig. S10). According to Turner et al. (57), $\beta_{GPP-SIF}$ are 9.1 and 11.0 for grasslands and nongrasslands, respectively, with corresponding SEs ($\sigma\beta_{GPP-SIF}$) of 0.2 and 0.3, respectively. $\beta_{NEE-GPP}$ is determined as the OLS regression coefficient in Eq. **5** (*SI Appendix*, Table S2 and Fig. S21) and $\sigma\beta_{SNEE-GPP}$ represents the associated SE of the coefficient (*SI Appendix*, Table S2). When sampling $fPAR_{growing}$, we use the mean value of 0.2 and the SD of 0.05, ensuring that 95% of the samples fall within the range of 0.1 to 0.3. Based on 1,000 bootstrap samples, we calculate the median and the 90% CI using the 5th and 95th percentiles, as shown in Fig. 4.

Data, Materials, and Software Availability. The TROPOMI SIF product can be accessed at https://climatesciences.jpl.nasa.gov/sif/download-data/level-2/ (34). Hourly meteorological data from ERA5 is publicly available through the Copernicus Climate Change Service (https://cds.climate.copernicus.eu/cdsapp#!/dataset/reanalysis-era5-single-levels?tab=form) (78). VIIRS EPS AOD data can be downloaded from https://www.star.nesdis.noaa.gov/pub/smcd/VIIRS_Aerosol/viirs_aerosol_gridded_data/ (79). The MODIS MCD12Q1 v006 landcover data are available at https://lpdaac.usgs.gov/products/mcd12q1v006/ (80). Additionally, the MODIS MOD15A2H v006 fPAR data can be found at https://lpdaac.usgs.gov/products/mod15a2hv006/ (81). The MODIS MCD18C2 v061 PAR data are available at https://lpdaac.usgs.gov/products/mcd18c2v061/ (82). FLUXCOM GPP and NEE are available at https://www.fluxcom.org/CF-Download/ (76). TROPOMI NO_2 can be downloaded from http://www.tropomi.eu/data-products/nitrogen-dioxide (83). MODIS cloud optical thickness is available at https://ladsweb.modaps.eosdis.nasa.gov/missions-and-measurements/products/MCD06COSP_D3_MODIS (84). The eddy covariance measurements are obtained from the ICOS (https://meta.icos-cp.eu/collections/-ZrCo_Cousoqvxnlvz83l0K4) (72). The SEM analysis is carried out using the "semopy" package in Python. The regression analysis is conducted by "statsmodels" package in Python. All other data are included in the manuscript and/or *SI Appendix*.

ACKNOWLEDGMENTS. This work was supported by the Carnegie Institution for Science. L.H. was partially supported by the fellowship from Resnick

Sustainability Institute at California Institute of Technology. Y. Yin and C.F. were supported by the NASA OCO2/3 science team (Grant 80NSSC18K0895). Y.W. was supported by the NSF grant (Award No. AGS-2103714). We thank Drs. Wu Sun (Carnegie Institution for Science), Yujie Wang (California Institute of Technology), and Xinchen Lu (University of California, Berkeley) for helpful discussions.

Author affiliations: [a]Department of Global Ecology, Carnegie Institution for Science, Stanford, CA 94305; [b]Department of Earth System Science, Stanford University, Stanford, CA 94305; [c]Center on Food Security and the Environment, Stanford University, Stanford, CA 94305; [d]Division of Geological and Planetary Sciences, California Institute of Technology, Pasadena, CA 91125; [e]Department of Environmental Studies, New York University, New York, NY 10003; [f]College of Atmospheric and Geographic Sciences, University of Oklahoma, Norman, OK 73019; and [g]Jet Propulsion Laboratory, California Institute of Technology, Pasadena, CA 91109

1. IPCC, "Climate change 2022: Mitigation of climate change" in *Contribution of Working Group III to the Sixth Assessment Report of the Intergovernmental Panel on Climate Change*, P. R. Shukla *et al.*, Eds. (Cambridge University Press, Cambridge, UK/New York, NY, 2022). https://doi.org/10.1017/9781009157926.
2. M. O. Andreae, D. Rosenfeld, Aerosol–cloud–precipitation interactions. Part 1. The nature and sources of cloud-active aerosols. *Earth Sci. Rev.* **89**, 13–41 (2008).
3. K. S. Hemes, J. Verfaillie, D. D. Baldocchi, Wildfire-smoke aerosols lead to increased light use efficiency among agricultural and restored wetland land uses in California's central valley. *J. Geophys. Res. Biogeosci.* **125**, e2019JG005380 (2020).
4. L. Gu *et al.*, Response of a deciduous forest to the Mount Pinatubo eruption: Enhanced photosynthesis. *Science* **1979**, 2035–2038 (2003).
5. S. A. W. Gerstl, A. Zardecki, Effects of aerosols on photosynthesis. *Nature* **300**, 436–437 (1982).
6. K. D. Kanniah, J. Beringer, P. North, L. Hutley, Control of atmospheric particles on diffuse radiation and terrestrial plant productivity: A review. *Prog. Phys. Geogr.* **36**, 209–237 (2012).
7. T. Matsui, A. Beltrán-Przekurat, D. Niyogi, R. A. Pielke Sr., M. Coughenour, Aerosol light scattering effect on terrestrial plant productivity and energy fluxes over the eastern United States. *J. Geophys. Res.: Atmos.* **113**, D14S14 (2008).
8. X. Wang *et al.*, Intermediate aerosol loading enhances photosynthetic activity of croplands. *Geophys. Res. Lett.* **48**, e2020GL091893 (2021).
9. X. Wang *et al.*, Field evidences for the positive effects of aerosols on tree growth. *Global Change Biol.* **24**, 4983–4992 (2018).
10. X. Yue, N. Unger, Aerosol optical depth thresholds as a tool to assess diffuse radiation fertilization of the land carbon uptake in China. *Atmos. Chem. Phys.* **17**, 1329–1342 (2017).
11. J. Zhang *et al.*, Effects of increasing aerosol optical depth on the gross primary productivity in China during 2000–2014. *Ecol. Indic.* **108**, 105761 (2020).
12. X. Tie *et al.*, Effect of heavy haze and aerosol pollution on rice and wheat productions in China. *Sci. Rep.* **6**, 1–6 (2016).
13. Y. Zhang *et al.*, Increased global land carbon sink due to aerosol-induced cooling. *Global Biogeochem. Cycles* **33**, 439–457 (2019).
14. J. Proctor, S. Hsiang, J. Burney, M. Burke, W. Schlenker, Estimating global agricultural effects of geoengineering using volcanic eruptions. *Nature* **560**, 480–483 (2018).
15. J. Pongratz, D. B. Lobell, L. Cao, K. Caldeira, Crop yields in a geoengineered climate. *Nat. Clim. Change* **2**, 101–105 (2012).
16. S. Liu, M. Chen, Q. Zhuang, Direct radiative effects of tropospheric aerosols on changes of global surface soil moisture. *Clim. Change* **136**, 175–187 (2016).
17. S. Liu, M. Chen, Q. Zhuang, Aerosol effects on global land surface energy fluxes during 2003–2010. *Geophys. Res. Lett.* **41**, 7875–7881 (2014).
18. Y. Wang *et al.*, Reduced European aerosol emissions suppress winter extremes over northern Eurasia. *Nat. Clim. Change* **10**, 225–230 (2020).
19. J. Burney, V. Ramanathan, Recent climate and air pollution impacts on indian agriculture. *Proc. Natl. Acad. Sci. U.S.A.* **111**, 16319–16324 (2014).
20. W. L. Chameides *et al.*, Case study of the effects of atmospheric aerosols and regional haze on agriculture: An opportunity to enhance crop yields in China through emission controls? *Proc. Natl. Acad. Sci. U.S.A.* **96**, 13626–13633 (1999).
21. L. He *et al.*, Marked impacts of pollution mitigation on crop yields in China. *Earth's Future* **10**, e2022EF002936 (2022).
22. X. Liu, A. R. Desai, Significant reductions in crop yields from air pollution and heat stress in the United States. *Earth's Future* **9**, e2021EF002000 (2021).
23. M. Chen, Q. Zhuang, Evaluating aerosol direct radiative effects on global terrestrial ecosystem carbon dynamics from 2003 to 2010. *Tellus B: Chem. Phys. Meteorol.* **66**, 21808 (2014).
24. X. Xie *et al.*, Effects of atmospheric aerosols on terrestrial carbon fluxes and CO_2 concentrations in China. *Atmos. Res.* **237**, 104859 (2020).
25. H. Zhou *et al.*, Responses of gross primary productivity to diffuse radiation at global FLUXNET sites. *Atmos. Environ.* **244**, 117905 (2021).
26. D. Niyogi *et al.*, Direct observations of the effects of aerosol loading on net ecosystem CO_2 exchanges over different landscapes. *Geophys. Res. Lett.* **31**, L20506 (2004).
27. S. Strada, N. Unger, X. Yue, Observed aerosol-induced radiative effect on plant productivity in the eastern United States. *Atmos. Environ.* **122**, 463–476 (2015).
28. G. G. Cirino, R. A. F. Souza, D. K. Adams, P. Artaxo, The effect of atmospheric aerosol particles and clouds on net ecosystem exchange in the Amazon. *Atmos. Chem. Phys.* **14**, 6523–6543 (2014).
29. E. Ezhova *et al.*, Direct effect of aerosols on solar radiation and gross primary production in boreal and hemiboreal forests. *Atmos. Chem. Phys.* **18**, 17863–17881 (2018).
30. S.-B. Park *et al.*, Strong radiative effect induced by clouds and smoke on forest net ecosystem productivity in central Siberia. *Agric. For. Meteorol.* **250**, 376–387 (2018).
31. Z. Zhang *et al.*, Satellite-observed vegetation responses to aerosols variability. *Agric. For. Meteorol.* **329**, 109278 (2023).
32. D. S. Moreira *et al.*, Modeling the radiative effects of biomass burning aerosols on carbon fluxes in the Amazon region. *Atmos. Chem. Phys.* **17**, 14785–14810 (2017).
33. M. S. Lee *et al.*, Model-based analysis of the impact of diffuse radiation on CO_2 exchange in a temperate deciduous forest. *Agric. For. Meteorol.* **249**, 377–389 (2018).
34. P. Köhler *et al.*, Global retrievals of solar-induced chlorophyll fluorescence with TROPOMI: First results and intersensor comparison to OCO-2. *Geophys. Res. Lett.* **45**, 10–456 (2018).
35. L. He *et al.*, Tracking seasonal and interannual variability in photosynthetic downregulation in response to water stress at a temperate deciduous forest. *J. Geophys. Res. Biogeosci.* **125**, e2018JG005002 (2020).
36. Y. Sun *et al.*, OCO-2 advances photosynthesis observation from space via solar-induced chlorophyll fluorescence. *Science* **358**, eaam5747 (2017).
37. C. Frankenberg *et al.*, New global observations of the terrestrial carbon cycle from GOSAT: Patterns of plant fluorescence with gross primary productivity. *Geophys. Res. Lett.* **38**, L17706 (2011).
38. X. Li, J. Xiao, B. He, Chlorophyll fluorescence observed by OCO-2 is strongly related to gross primary productivity estimated from flux towers in temperate forests. *Remote Sens. Environ.* **204**, 659–671 (2018).
39. Y. Zhang *et al.*, Consistency between sun-induced chlorophyll fluorescence and gross primary production of vegetation in North America. *Remote Sens. Environ.* **183**, 154–169 (2016).
40. R. Doughty *et al.*, Global-scale consistency of spaceborne vegetation indices, chlorophyll fluorescence, and photosynthesis. *J. Geophys. Res. Biogeosci.* **126**, e2020JG006136 (2021).
41. L. Guanter *et al.*, Global and time-resolved monitoring of crop photosynthesis with chlorophyll fluorescence. *Proc. Natl. Acad. Sci. U.S.A.* **111**, E1327–E1333 (2014).
42. J. Joiner, Y. Yoshida, A. P. Vasilkov, E. M. Middleton, First observations of global and seasonal terrestrial chlorophyll fluorescence from space. *Biogeosciences* **8**, 637–651 (2011).
43. C. Frankenberg, C. O'Dell, L. Guanter, J. McDuffie, Remote sensing of near-infrared chlorophyll fluorescence from space in scattering atmospheres: Implications for its retrieval and interferences with atmospheric CO_2 retrievals. *Atmos. Meas. Tech.* **5**, 2081–2094 (2012).
44. R. Houborg, M. F. McCabe, Impacts of dust aerosol and adjacency effects on the accuracy of Landsat 8 and RapidEye surface reflectances. *Remote Sens. Environ.* **194**, 127–145 (2017).
45. G. Forzieri *et al.*, Emergent vulnerability to climate-driven disturbances in European forests. *Nat. Commun.* **12**, 1081 (2021).
46. R. Matyssek *et al.*, Forests under climate change and air pollution: Gaps in understanding and future directions for research. *Environ. Pollut.* **160**, 57–65 (2012).
47. European Commission, *Climate Change–Restoring Sustainable Carbon Cycles* (European Commission, 2021).
48. A. K. Georgoulias, K. A. Kourtidis, A high resolution satellite view of the aerosol weekly cycle variability over Central Europe. *Atmos. Res.* **107**, 145–160 (2012).
49. X. Xia, T. F. Eck, B. N. Holben, G. Phillippe, H. Chen, Analysis of the weekly cycle of aerosol optical depth using AERONET and MODIS data. *J. Geophys. Res.: Atmos.* **113**, D14217 (2008).
50. A. K. Georgoulias, K. A. Kourtidis, On the aerosol weekly cycle spatiotemporal variability over Europe. *Atmos. Chem. Phys.* **11**, 4611–4632 (2011).
51. Y. Fan *et al.*, Applications of structural equation modeling (SEM) in ecological studies: An updated review. *Ecol. Process.* **5**, 1–12 (2016).
52. L. Gu *et al.*, Advantages of diffuse radiation for terrestrial ecosystem productivity. *J. Geophys. Res.: Atmos.* **107**, ACL-2 (2002).
53. P. B. Alton, P. R. North, S. O. Los, The impact of diffuse sunlight on canopy light-use efficiency, gross photosynthetic product and net ecosystem exchange in three forest biomes. *Global Change Biol.* **13**, 776–787 (2007).
54. T. S. Magney, M. L. Barnes, X. Yang, On the covariation of chlorophyll fluorescence and photosynthesis across scales. *Geophys. Res. Lett.* **47**, e2020GL091098 (2020).
55. Y. Sun *et al.*, From remotely-sensed SIF to ecosystem structure, function, and service: Part II–Harnessing data. *Global Change Biol.* **29**, 2926–2952 (2023).
56. X. Li, J. Xiao, TROPOMI observations allow for robust exploration of the relationship between solar-induced chlorophyll fluorescence and terrestrial gross primary production. *Remote Sens. Environ.* **268**, 112748 (2022).
57. A. J. Turner *et al.*, Extreme events driving year-to-year differences in gross primary productivity across the US. *Biogeosciences* **18**, 6579–6588 (2021).
58. Z. S. Venter, K. Aunan, S. Chowdhury, J. Lelieveld, COVID-19 lockdowns cause global air pollution declines. *Proc. Natl. Acad. Sci. U.S.A.* **117**, 18984–18990 (2020).
59. L. Rosa, M. Mazzotti, Potential for hydrogen production from sustainable biomass with carbon capture and storage. *Renewable Sustainable Energy Rev.* **157**, 112123 (2022).
60. L. Rosa, D. L. Sanchez, M. Mazzotti, Assessment of carbon dioxide removal potential via BECCS in a carbon-neutral Europe. *Energy Environ. Sci.* **14**, 3086–3097 (2021).
61. T. Terlouw, C. Bauer, L. Rosa, M. Mazzotti, Life cycle assessment of carbon dioxide removal technologies: A critical review. *Energy Environ. Sci.* **14**, 1701–1721 (2021).
62. P. Gabrielli *et al.*, Net-zero emissions chemical industry in a world of limited resources. *One Earth* **6**, 682–704 (2023).
63. L. Rosa, P. Gabrielli, Achieving net-zero emissions in agriculture: A review. *Environ. Res. Lett.* **18**, 063002 (2023).
64. K. Caldeira, G. Bala, L. Cao, The science of geoengineering. *Annu. Rev. Earth Planet Sci.* **41**, 231–256 (2013).
65. F. Su *et al.*, Rapid greening response of China's 2020 spring vegetation to COVID-19 restrictions: Implications for climate change. *Sci. Adv.* **7**, eabe8044 (2021).
66. R. Kashyap, J. Kuttippurath, V. K. Patel, Improved air quality leads to enhanced vegetation growth during the COVID–19 lockdown in India. *Appl. Geogr.* **151**, 102869 (2023).
67. L. He *et al.*, From the ground to space: Using solar-induced chlorophyll fluorescence to estimate crop productivity. *Geophys. Res. Lett.* **47**, e2020GL087474 (2020).
68. A. J. Turner *et al.*, A double peak in the seasonality of California's photosynthesis as observed from space. *Biogeosciences* **17**, 405–422 (2020).
69. R. Doughty *et al.*, TROPOMI reveals dry-season increase of solar-induced chlorophyll fluorescence in the Amazon forest. *Proc. Natl. Acad. Sci. U.S.A.* **116**, 22393–22398 (2019).
70. L. Guanter *et al.*, The TROPOSIF global sun-induced fluorescence dataset from the Sentinel-5P TROPOMI mission. *Earth Syst. Sci. Data* **13**, 5423–5440 (2021).
71. C. Li *et al.*, Evaluating VIIRS EPS Aerosol Optical Depth in China: An intercomparison against ground-based measurements and MODIS. *J. Quant. Spectrosc. Radiat. Transf.* **224**, 368–377 (2019).

72. ICOS RI, *Ecosystem Final Quality (L2) Product in ETC-Archive Format–Release 2022-1. (Version 1.0). ICOS ERIC–Carbon Portal* (ICOS RI, 2022), https://doi.org/10.18160/PAD9-HQHU.
73. G. Pastorello *et al.*, The FLUXNET2015 dataset and the ONEFlux processing pipeline for eddy covariance data. *Sci. Data* **7**, 1–27 (2020).
74. Y. Yin *et al.*, Cropland carbon uptake delayed and reduced by 2019 Midwest floods. *AGU Adv.* **1**, e2019AV000140 (2020).
75. X. Li *et al.*, Solar-induced chlorophyll fluorescence is strongly correlated with terrestrial photosynthesis for a wide variety of biomes: First global analysis based on OCO-2 and flux tower observations. *Global Change Biol.* **24**, 3990–4008 (2018), https://doi.org/10.1111/gcb.14297.
76. M. Jung *et al.*, Scaling carbon fluxes from eddy covariance sites to globe: Synthesis and evaluation of the FLUXCOM approach. *Biogeosciences* **17**, 1343–1365 (2020).
77. Z. Zhang, J. M. Chen, L. Guanter, L. He, Y. Zhang, From canopy-leaving to total canopy far-red fluorescence emission for remote sensing of photosynthesis: First results from TROPOMI. *Geophys. Res. Lett.* **46**, 12030–12040 (2019).
78. H. Hersbach *et al.*, ERA5 hourly data on single levels from 1940 to present. Copernicus Climate Change Service (C3S) Climate Data Store (CDS). https://doi.org/10.24381/cds.adbb2d47. Accessed 15 March 2022.
79. I. Laszlo, H. Liu, EPS aerosol optical depth (AOD) algorithm theoretical basis document. SNPP VIIRS Aerosol Optical Depth Gridded Reprocessed. https://www.star.nesdis.noaa.gov/pub/smcd/VIIRS_Aerosol/viirs_aerosol_gridded_data/. Accessed 15 March 2022.
80. M. Friedl, D. Sulla-Menashe, MCD12Q1 MODIS/Terra+Aqua Land Cover Type Yearly L3 Global 500m SIN Grid V006 [Data set]. NASA EOSDIS Land Processes Distributed Active Archive Center. https://doi.org/10.5067/MODIS/MCD12Q1.006. Accessed 15 March 2022.
81. R. Myneni, Y. Knyazikhin, T. Park, MOD15A2H MODIS/Terra Leaf Area Index/FPAR 8-Day L4 Global 500m SIN Grid V006 [Data set]. NASA EOSDIS Land Processes Distributed Active Archive Center. https://doi.org/10.5067/MODIS/MOD15A2H.006. Accessed 15 March 2022.
82. D. Wang, MODIS/Terra+Aqua Photosynthetically Active Radiation Daily/3-Hour L3 Global 0.05 Deg CMG V061 [Data set]. NASA EOSDIS Land Processes Distributed Active Archive Center. https://doi.org/10.5067/MODIS/MCD18C2.061. Accessed 15 March 2022.
83. European Space Agency, TROPOMI level 2 nitrogen dioxide total column products. Version 02. Copernicus Sentinel-5P data products. https://doi.org/10.5270/S5P-9bnp8q8. Accessed 15 March 2022.
84. Level-1 and Atmosphere Archive & Distribution System, MCD06COSP_D3_MODIS – MODIS (Aqua/Terra) Cloud Properties Level 3 Daily, 1x1 Degree Grid. NASA [data set]. https://doi.org/10.5067/MODIS/MCD06COSP_D3_MODIS.062. Accessed 15 March 2022.